Applied Catalysis B: Environmental 148–149 (2014) 258–268

Contents lists available at ScienceDirect

Applied Catalysis B: Environmental

journal homepage: www.elsevier.com/locate/apcatb

Sunlight photocatalytic activity enhancement and mechanism of novel europium-doped ZnO hierarchical micro/nanospheres for degradation of phenol

Jin-Chung Sin [a], Sze-Mun Lam [a], Ichikawa Satoshi [b], Keat-Teong Lee [a], Abdul Rahman Mohamed [a,*]

[a] School of Chemical Engineering, Universiti Sains Malaysia, Engineering Campus, 14300 Nibong Tebal, Pulau Pinang, Malaysia
[b] Institute for NanoScience Design, Osaka University, 1-3 Machikaneyama, Toyonaka, Osaka, Japan

ARTICLE INFO

Article history:
Received 14 August 2013
Received in revised form 31 October 2013
Accepted 3 November 2013
Available online 10 November 2013

Keywords:
ZnO
Europium
Doping
Hierarchical
Photocatalysis

ABSTRACT

Europium-doped ZnO hierarchical micro/nanospheres (Eu/ZnO) were synthesized for the first time via a facile and surfactant-free chemical solution route. The as-synthesized products were characterized by X-ray diffraction, field-emission scanning electron microscopy, energy dispersion X-ray analysis, transmission electron microscopy, high-resolution transmission electron microscopy, X-ray photoelectron spectroscopy, UV–visible diffuse reflectance spectroscopy, nitrogen adsorption–desorption and photoluminescence spectroscopy. The results showed that the as-synthesized products were well-crystalline and accumulated by large amount of interleaving nanosheets. It was also observed that the Eu doping increased the light absorption ability of Eu/ZnO and a red shift for Eu/ZnO appeared when compared to pure ZnO. Under natural sunlight irradiation, the Eu/ZnO exhibited much higher photocatalytic activity than those of pure ZnO, Eu-doped ZnO nanorods (Eu/ZNRs) and commercial TiO_2 for the degradation of phenol. The photocatalytic enhancement of Eu/ZnO products was attributed to their high charge separation efficiency and hydroxyl radical generation ability as evidenced by the photoluminescence spectra. By using several radical scavengers, hydroxyl radical was determined to play a pivotal role for the phenol degradation. Furthermore, the Eu/ZnO could be easily separated and reused, showing great potential for practical applications in environmental cleanup and solar energy conversion.

1. Introduction

During the last two decades, different applications for advanced science and technology relating to industrial processes and agricultural productions have led to considerably increase in a number of phenols, pesticides, dyes, solvents and other organic pollutants existing in various natural resources. Most of them were resistant to biodegradation and may undergo natural reductive anaerobic degradation to yield potentially carcinogenic intermediates [1]. The photocatalytic reaction has become a desirable method to transform the organic pollutants into nontoxic molecules to eliminate the environmental pollution. Many oxide semiconductors, such as ZnO [2–4], TiO_2 [1,5], Ag_3PO_4 [6], WO_3 [7] and Bi_2O_3 [8] have been reported as significant photocatalytic materials in various organic pollutants degradation and antimicrobial application. ZnO is a wide band gap (~3.3 eV) semiconductor which has been extensively used because of its catalytic and photochemical properties along with its low cost [3]. Moreover, there are many reports of ZnO having higher photocatalytic activities than other semiconductors in both air and aqueous media [9,10].

The surface area of the photocatalyst played a significant role because the photocatalytic reactions mainly occurred at the interface between the catalyst surfaces and organic pollutants. The nanoscale ZnO has shown the larger specific surface area-to-volume ratio and higher photocatalyic performance than that of bulk materials [11]. Much effort has been devoted to the synthesis of nanostructured ZnO with tunable size and shape parameter to effectively degrade numerous pollutants in the wastewaters [11–13]. However, it should be mentioned that the low dimensional nanoscaled building blocks (such as nanoparticles, nanorods and nanosheets) tend to aggregate during the preparation and photocatalysis processes, resulting in reduction of their surface area and photocatalytic efficiency. Therefore, three-dimensional (3D) semiconductor materials with hierarchical structure have aroused great concern due to their fine structure and larger size that can avoid the aggregation of particles during application as photocatalysts [4,14]. For example, flower-like ZnO hierarchical microarchitectures exhibited an enhanced photocatalytic

* Corresponding author. Tel.: +60 45996410; fax: +60 45941013.
E-mail address: chrahman@eng.usm.my (A.R. Mohamed).

0926-3373/$ – see front matter © 2013 Elsevier B.V. All rights reserved.
http://dx.doi.org/10.1016/j.apcatb.2013.11.001

performance compared with the other nanostructured ZnO powders of nanoparticles, nanorods and nanosheets [4]. Hitherto, most of 3D hierarchical structures were developed via the surfactants or structure-directing reagents assisted route, and assemblage of nanoscaled building blocks into the 3D structured morphologies without any surfactants still remains an intricate challenge.

The solar energy utilization efficiency could be improved by modifying the ZnO through doping of metal or non-metal ions, deposition of noble metals as well as use of coupled semiconductors [15–17]. Recently, some studies have reported ZnO doping with rare earth (RE) ions showed enhancement in light absorption due to the creation of impurity energy levels within the band gap [18,19]. Moreover, RE ions doping produced traps for photogenerated charge carriers, thus lowering the electron-hole pairs recombination rate leading to an increase in the photocatalytic efficiency in ZnO [16,18]. Khatamian et al. [18] reported that doping with La^{3+}, Nd^{3+} and Sm^{3+} improved the photoactivity of ZnO in degradation of 4-nitrophenol under UV irradiation. A study by Karunakaran et al. [19] also showed that the doping of Ce ions in ZnO enhanced the photooxidation of cyanide under solar irradiation. In fact, doping of ZnO is a subject of broad interest for the past few years. To the best of our knowledge, however, the doping of RE ions particularly Eu^{3+} in ZnO and their photocatalytic activities under natural sunlight irradiation have never been reported so far.

On the basis of the above consideration, this work reports for the first time on the synthesis of Eu-doped ZnO hierarchical micro/nanospheres (Eu/ZnO) by a simple chemical solution route without any organic solvent or surfactant. The morphology evolution and mechanism on the formation of the 3D ZnO hierarchical structure were investigated. The as-synthesized ZnO products were characterized by different techniques and used for the photocatalytic degradation of phenol under natural sunlight irradiation. Moreover, the stability of as-synthesized Eu/ZnO was studied through successive four cycles of experiments. The mechanism for the enhanced photoactivity of Eu/ZnO was finally discussed based on the separation process of electron-hole pairs and the active species detection.

2. Experimental

2.1. Preparation of Eu/ZnO

All the reagents used in this work were of analytical grade without further purification. The detailed synthesis procedure was as follows: 5.0 mmol zinc nitrate hexahydrate ($Zn(NO_3)_2{\cdot}6H_2O$) and europium (III) chloride hexahydrate ($Eu(Cl)_3{\cdot}6H_2O$) with different Eu/Zn ratios (0, 1.0, 1.5, 2.0, 3.0 at%) were dissolved in 80 mL of deionized water. Then 30 mmol NaOH was added into the above solution and stirred continuously for 3 h at room temperature. After stirring, the as-formed precipitates were filtrated, washed with deionized water for several times, dried at 60 °C in air for 12 h and finally calcined at 450 °C in air for 2 h.

2.2. Characterization

The products were characterized by X-ray diffraction (XRD) analysis on a Philips PW1820 diffractometer equipped with Cu Kα radiation over a range from 20 to 80°. The field-emission scanning electron microscopy (FESEM) was carried out using a Quanta FEG 450 together with an energy dispersion X-ray (EDX) analysis. Transmission electron microscopy (TEM) image was taken on a Philips CM 12 instrument operating at 120 keV. The high-resolution TEM (HRTEM) image was performed on a Tecnai 20. X-ray photoelectron spectroscopy (XPS) spectra were obtained with a XPS Omicron els 5000 spectrophotometer using Al Kα at 1480 kV as radiation X-ray source. Diffuse reflectance spectroscopy (DRS) of catalysts was tested in a Perkin Elmer Lambda 35 UV–vis spectrometer. The spectra were recorded timely in the range of 350–650 nm using $BaSO_4$ as the reference standard. The specific surface area and pore size distribution were obtained based on N_2 adsorption–desorption data using a Micromeritics ASAP 2020 instrument. Photoluminescence (PL) spectroscopy of synthesized products was taken at room temperature on a Perkin Elmer Lambda S55 spectrofluorometer using a Xe lamp with an excitation wavelength of 325 nm.

2.3. Measurement of photocatalytic activity

The photocatalytic activity of the as-synthesized ZnO products was evaluated by the degradation of phenol in water. The experiments were performed as follows: 100 mg catalyst was placed into 100 mL of 20 mg/L phenol aqueous solution in a beaker. During all experiments, air was bubbled into the solution at a constant flow rate of 6 mL/min. The suspensions were continuously stirred with the aid of a magnetic stirrer. The heterogeneous mixture was equilibrated for 1 h in the dark. Then, the solution was irradiated under natural sunlight. After the elapse of a period of time, 2 mL of the solution was withdrawn from the system, centrifuged and the concentration of the phenol at different time intervals was monitored by a HPLC (Perkin Elmer Series 200). The HPLC separations were performed at 254 nm with a mobile phase mixture of water and acetonitrile in the ratio of 70:30 (v/v) at a flow rate of 1 mL/min. All the photocatalytic experiments were performed on sunny days between 11:00 and 14:00 during the months of December and January. The average intensity of sunlight striking the surface of the reaction solution was about 90,000 lux, as measured by a digital luxmeter. Meanwhile, the comparison studies with commercial TiO_2 (100% anatase) and 2.0 at% Eu-doped ZnO nanorods (Eu(2.0 at%)/ZNRs) prepared by the solvothermal method according to our previous report [12] were also conducted. The total organic carbon (TOC) of degradation of phenol was measured using a Shimadzu TOC-V_{CPH} analyzer to determine the extent of mineralization.

The durability test of the as-synthesized ZnO products was also performed by using the same procedure as above and the product underwent four consecutive cycles, each lasting for 30 min. After each cycle, the catalyst was centrifuged and washed thoroughly with water, and then added to fresh phenol solution. In order to determine the reproducibility of all the results, at least duplicated runs were carried out for each condition for averaging the results, and the experimental error was found to be within ±4%.

2.4. Detection of active species

The roles of photogenerated positive charged hole (h_{vb}^+), hydroxyl radical (•OH) and superoxide anion radical ($O_2^{\bullet-}$) in the photocatalytic reactions were evaluated by adding 2 mM of different scavengers in a manner similar to the above photodegradation experiment. In a separate experiment, acetonitrile was used instead of water in order to confirm the role of •OH in the photocatalytic systems. Terephthalic acid photoluminescence (TA-PL) probing technique was also used in the detection of •OH. The detailed TA-PL experiment was similar to our previous report [20].

3. Results and discussion

3.1. Characterization of the as-synthesized products

Fig. 1 is the XRD patterns of as-synthesized products. The diffraction peaks of pure ZnO can be indexed to a hexagonal wurtzite structure (JCPDS file no. 36–1451). By doping 1.0–3.0 at% Eu in ZnO,

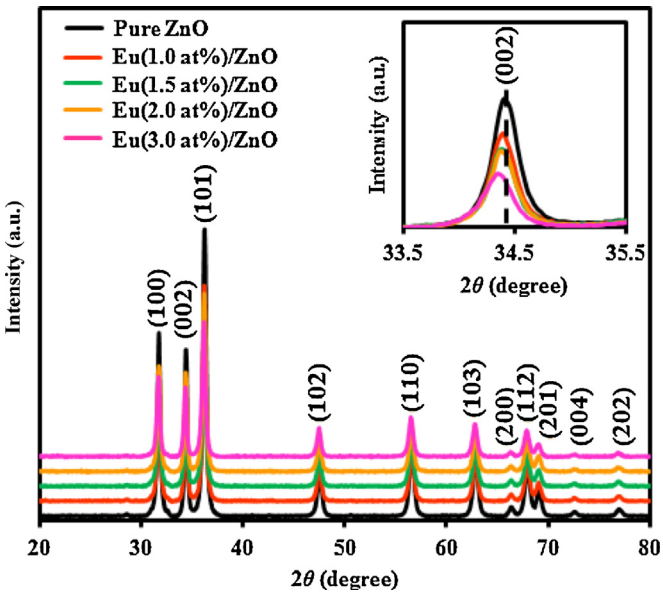

Fig. 1. XRD patterns of pure ZnO and Eu/ZnO with different doping contents of Eu. Inset is the magnified region of (0 0 2) peak.

their XRD patterns still the same as that of pure wurtzite ZnO structure and no other peaks corresponding to europium oxides or any other impurity phases were detected. To confirm the possible substitution of Zn ions with Eu ions in Eu/ZnO, the angle shift of 2θ for the ZnO (0 0 2) peak as a function of doping was observed. The position of the (0 0 2) peak of Eu/ZnO was slightly shifted toward the lower angles as Eu doping content rose from 0 to 3.0 at%, indicating the substitution of Eu partly in the crystalloid of ZnO. Similar shifts were reported before [21,22]. The slight increase of ZnO lattice parameters as a result of doping was also observed in Table 1 and was in agreement with the literature data for the possibility of Eu^{3+} (radius 0.095 nm) to replace Zn^{2+} (radius 0.074 nm) in the ZnO crystal [22]. Moreover, the diffraction peaks of ZnO became broader in width and weaker in intensity with increase in the nominal content of Eu, implying that Eu doping inhibited the growth of crystal size. The average crystallite sizes (D) of all the products were calculated with the (1 0 1) peak using Scherrer equation $D = 0.9\lambda/(\beta\cos\theta)$, where λ is the wavelength of the incident X-ray radiation, β is the full width at half maximum and θ is the Bragg angle. The calculated crystallite sizes of the doped products were slightly smaller than the pure ZnO and the results are also presented in Table 1. The decrease in the crystal size of Eu/ZnO was mainly attributed to the formation of Eu–O–Zn on the surface of the doped products, which inhibited the growth of crystal grains [23]. Similar inhibitory effect was also found for ZnO doped with various rare earth ions [23–25].

Fig. 2 shows the FESEM images of pure ZnO and Eu(2.0 at%)/ZnO. The panoramic morphologies of the products are presented in Fig. 2a and d, indicating the synthesized products were spherical-shaped and grown in large quantity. The sizes of micro/nanospheres were not uniform and varied from 870 nm to 2.80 μm. The magnified images in Fig. 2b and e showed that the microspheres presented a hierarchical structure. The high magnification FESEM images (Fig. 2c and f) clearly demonstrated that the surface structure of microspheres was accumulated by lots of nanosheets with average thickness of ~17 nm. The nanosheets intersected with each other,

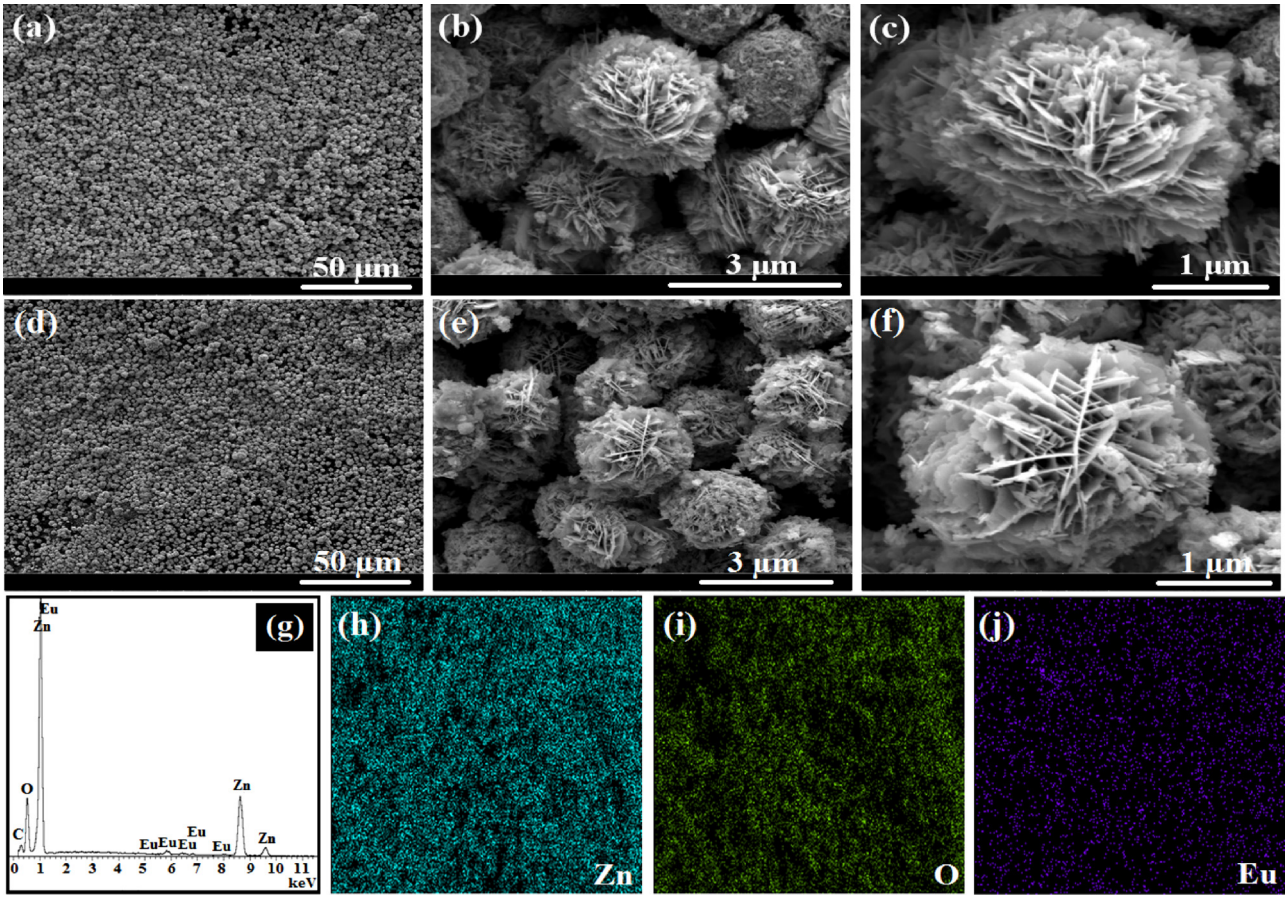

Fig. 2. (a–c) FESEM images of pure ZnO; (d–f) FESEM images of Eu(2.0 at%)/ZnO; (g) The EDX spectrum of Eu(2.0 at%)/ZnO and (h–j) The elemental mapping images of Eu(2.0 at%)/ZnO.

Table 1
Average crystallite size (D), lattice parameters, band gap energy (E_g) and the pseudo-first order rate constants (k) of different photocatalysts.

Product	$D_{(101)}$(nm)	Lattice parameter (a) nm	Lattice parameter (c) nm	E_g (eV)	k (min^{-1})
Pure ZnO	26	0.3249	0.5205	3.26	0.0379
Eu(1.0 at%)/ZnO	24	0.3249	0.5207	3.21	0.0584
Eu(1.5 at%)/ZnO	23	0.3249	0.5209	3.20	0.0791
Eu(2.0 at%)/ZnO	22	0.3250	0.5209	3.19	0.1236
Eu(3.0 at%)/ZnO	21	0.3250	0.5213	3.18	0.0650

which resulted in a net-like morphology with porous structure. Furthermore, doping of the ZnO hierarchical micro/nanospheres with Eu did not show any significant effect on the overall morphology. The elemental analysis of Eu(2.0 at%)/ZnO was identified using the EDX (Fig. 2g). The Zn, O and Eu peaks can be easily observed. The weak C peak was also detected, which originated from the supporting carbon tape. Furthermore, the EDX mapping of Eu(2.0 at%)/ZnO in Fig. 2h–j demonstrated that Zn, O and Eu ions were distributed homogeneously throughout the products.

Fig. 3a shows the TEM image of the synthesized Eu(2.0 at%)/ZnO, which is fully consistent with the FESEM observations in term of its morphologies and dimensionalities. The TEM image confirmed that the product with a diameter of about 2.8 μm was consisted of a large number of nanosheets. The observed TEM image also showed that many pores were formed in the nanosheets, which could be the result of loss of volatile gases such as H_2O and CO_2 during the heat treatment [26]. The porous feature of ZnO nanosheets in the Eu(2.0 at%)/ZnO was further confirmed by the corresponding HRTEM image (Fig. 3b). It was apparent that the pores with irregular shape of 4–13 nm were randomly distributed in the nanosheets. It was also noticeable that the ZnO products showed very clear lattice fringes with spacing of 0.26 nm between adjacent lattice planes corresponded to the d-spacing of the (0 0 2) plane of wurtzite structured ZnO. From the TEM and HRTEM images, it can be confirmed that the synthesized ZnO products have highly crystalline structure, which is essential for excellent photocatalytic materials.

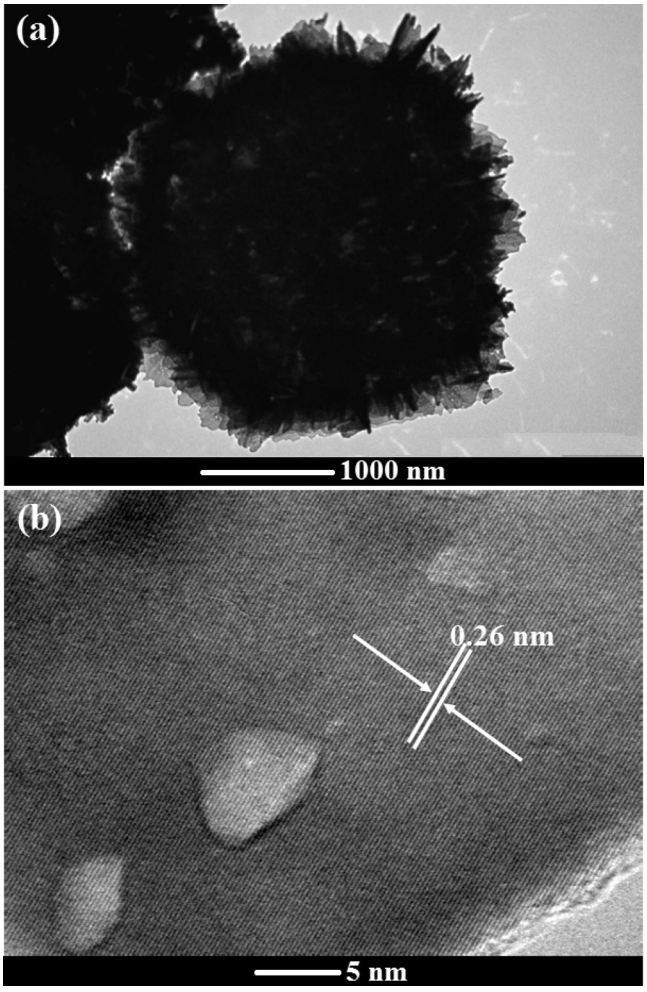

Fig. 3. (a) TEM and (b) HRTEM images of Eu(2.0 at%)/ZnO.

Fig. 4a shows the XPS spectrum of a Eu/ZnO with a Eu doping content of 2.0 at%. The products were composed of Zn, O and Eu elements, which further confirmed the doping of Eu within the ZnO matrix. A trace amount of carbon in the results was mainly attributed to the adventitious hydrocarbon from XPS itself [27]. Fig. 4b–d shows the high resolution XPS spectra of the elements of O, Zn and Eu. The O 1s region of the XPS spectrum can be fitted by two peaks at 530.3 eV and 532.1 eV as shown in Fig. 4b. An intense low-energy component at 530.3 eV was attributed to O^{2-} ions in ZnO and the high energy component at 532.1 eV can be ascribed to the hydroxyl species on the catalyst surface [27,28]. In Fig. 4c, the peaks located at 1022.9 eV and 1045.9 eV were associated to Zn $2p_{3/2}$ and Zn $2p_{1/2}$, respectively [29]. The Eu 3d region (Fig. 4d) was displayed with the characteristic peaks at 1135.8 eV and 1164.6 eV were ascribed to the core levels of Eu $3d_{5/2}$ and Eu $3d_{3/2}$, respectively, which indicated that the Eu ions were trivalent [30,31].

Fig. 5 shows the UV–vis DRS spectra of all the Eu/ZnO products along with the pure ZnO. Modification of ZnO with europium significantly affected the light absorption property of the photocatalysts. It was noticeable that the light absorption of Eu/ZnO in the visible light range was higher than that of pure ZnO and the light absorption increased with increasing the Eu content. Furthermore, a slight red shift of the optical absorption edge was observed for all the doped products compared to pure ZnO. The observed red shift indicated the narrower band gap originated from the charge transfer between the ZnO valence band and the Eu ion 4f level [32]. It has already been reported that the doping of RE can form discrete empty energy levels below the conduction band of crystalline ZnO. Their presence allowed a new electronic transition from the ZnO valence band to the empty energy levels of RE with less energy than ZnO valence-conduction band transition [18,33,34]. Thus, the red shift was observed in the Eu/ZnO products as compared to pure ZnO. The band gap energies of as-synthesized ZnO products were calculated according to the equation E_g (eV) = $hc/\lambda = 1240/\lambda$ (nm), where E_g is the band gap energy (eV), h is the Planck's constant (4.135667×10^{-15} eVs), c is the velocity of light (3×10^8 m/s) and λ is the wavelength (nm) of absorption onset. Using the equation, the measured band gap energies of the doped products were lower than the pure ZnO and the results are shown in Table 1. Above results revealed that the Eu/ZnO can absorb in UV as well as in visible region of the solar light. Hence, the absorption property deduced that the Eu/ZnO could be promising in sunlight photocatalysis.

3.2. Formation of the 3D hierarchical micro/nanospheres

To understand the formation process of hierarchical micro/nanospheres, time-dependent morphology evolution

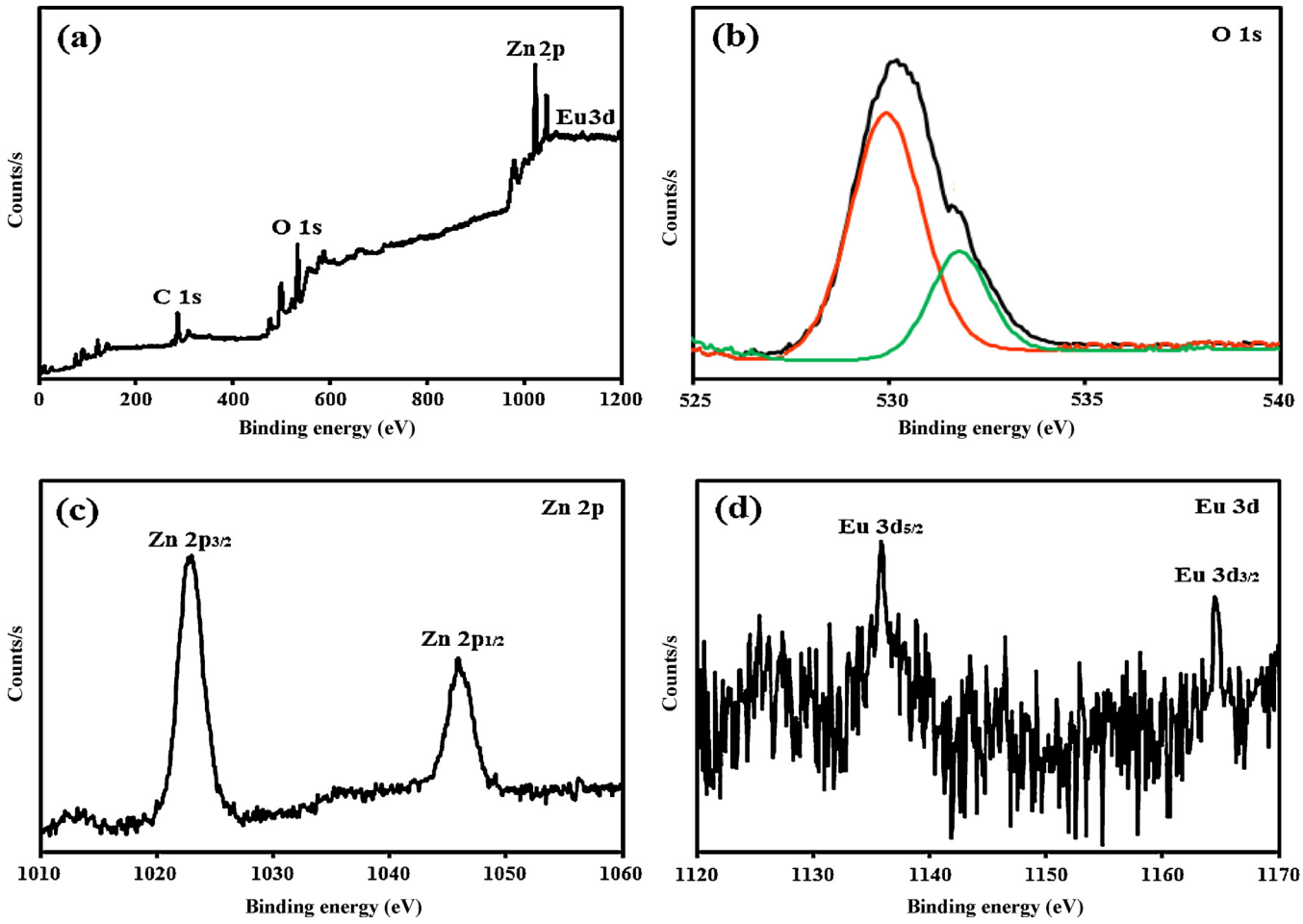

Fig. 4. XPS spectra of Eu(2.0 at%)/ZnO: (a) survey; (b) O 1 s peaks; (c) Zn 2p peaks and (d) Eu 3d peaks.

experiments were carried out and the products prepared at different reaction times were examined by FESEM. As shown in Fig. 6a, spherical microparticles accompanying small nanoparticles were obtained at early stage (5 min). When the reaction time was prolonged to 30 min, more spherical microparticles were formed due to Ostwald ripening. Meanwhile, the hierarchical micro/nanospheres, which consisted of many nanosheets were produced (Fig. 6b). When the reaction time was further up to 90 min, more hierarchical micro/nanospheres were obtained (Fig. 6c). With an extension of the reaction time to 180 min, the products were composed of mostly well shaped hierarchical micro/nanospheres (Fig. 6d).

On the basis of studies mentioned above, it can be concluded that the formation of such hierarchical structure was achieved via a two-stage nucleation-growth process. Scheme 1 shows the whole formation process of hierarchical micro/nanospheres. When NaOH was introduced into the Zn^{2+} aqueous solution, reactions can occur as follows:

$$Zn^{2+} + 2OH^- \rightarrow Zn(OH)_2\downarrow \quad (1)$$

$$Zn(OH)_2 + 2OH^- \rightarrow Zn(OH)_4{}^{2-} \quad (2)$$

$$Zn(OH)_4{}^{2-} \rightarrow ZnO + H_2O + 2OH^- \quad (3)$$

Firstly, $Zn(OH)_2$ precipitate was obtained when adding alkali into the Zn^{2+} solution, and the $Zn(OH)_2$ precipitate was successively dissolved to yield a homogeneous aqueous solution containing $Zn(OH)_4{}^{2-}$ ions. Upon increasing the time further, ZnO nuclei were formed from the dehydration of $Zn(OH)_4{}^{2-}$ ions and followed by the crystal growth. During this process, a burst of initial homogeneous nucleation happened and the tiny crystalline nuclei were generated in a supersaturated solution and then led to the formation of ZnO nanoclusters. With the reaction proceeding, these ZnO nanoclusters would aggregate to minimize their surface area, which resulted in the formation of numerous spherical

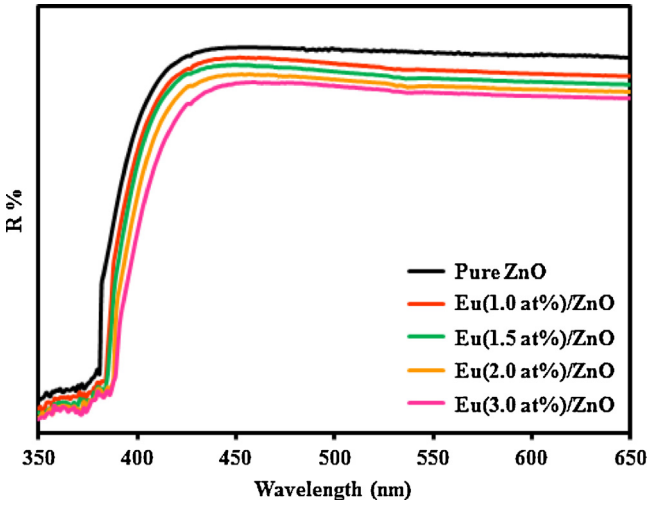

Fig. 5. UV–vis DRS spectra of pure ZnO and Eu/ZnO with different doping contents of Eu.

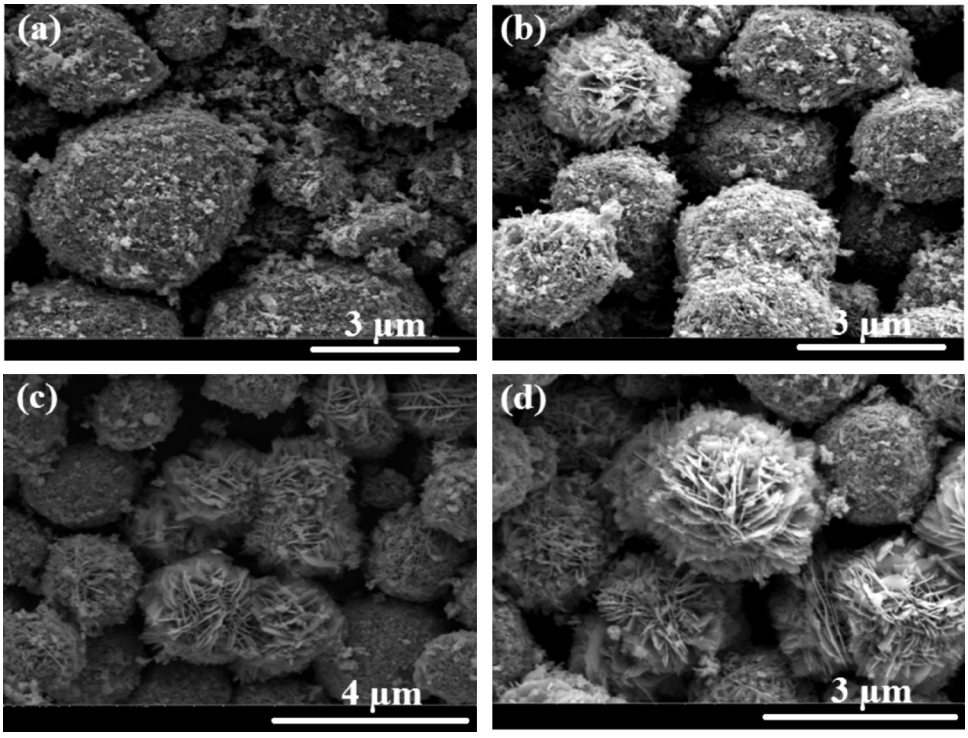

Fig. 6. FESEM images of the products collected at different growth stages: (a) 5 min; (b) 30 min; (c) 90 min and (d) 180 min.

microparticles through the process known as Ostwald ripening [35]. After that, these aggregated spherical microparticles could serve as the sites for the growth of primary ZnO nanosheets. The surface of primary ZnO nanosheets formed during the initial growth stage has many crystalline boundaries and was thermodynamically unstable. They would tend to further decrease their energy through surface reconstruction [36], which would provide active sites for secondary heterogeneous nucleation and growth. Therefore, the secondary nanosheets would grow out continuously from the surface of the primary ones, which interlaced and overlapped with each other into a discernible multilayer and network structure to constitute the hierarchical ZnO micro/nanospheres. In our work, the 3D ZnO structures with nanosheets were fabricated without any surfactant and structure-directing reagents, and it is also a facile way for large-scale synthesis of 3D ZnO structures.

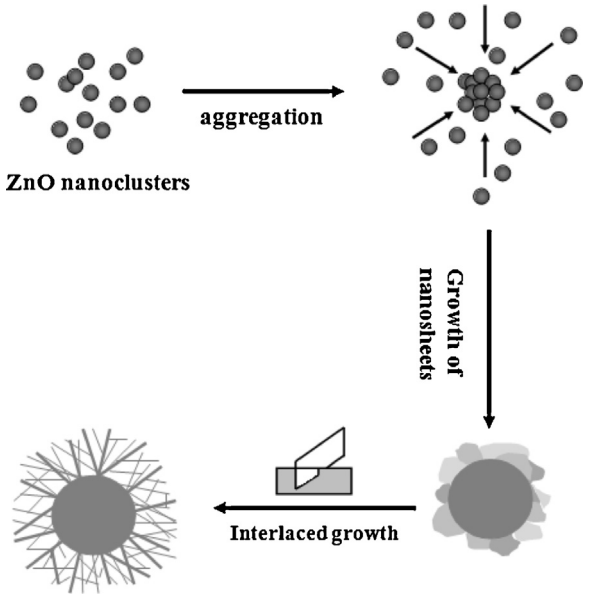

Scheme 1. Schematic illustration of the formation process of ZnO hierarchical micro/nanospheres.

3.3. Photocatalytic activity

The photocatalytic activities of the as-synthesized ZnO products were evaluated by the degradation of phenol aqueous solution. Phenol is an endocrine disrupting chemical which produced worldwide in millions of tons each year and widely used in manufacturing of resins, insulation panels, pesticides, paints and lubricants [37]. The extensive use and poor biodegradability of phenol have resulted in its ubiquitous presence in the environment. Widespread occurrences of phenol in surface waters have been reported in several countries at concentrations ranging from <1 to 7.8 μg/L [38,39]. Evidence of phenol effect came from observation of increased chromosome aberrations in spermatogonia and primary spermatocytes of mice treated with a solution of phenol in water [40]. Thus, phenol was chosen as the model substrate to evaluate the photocatalytic activities of the as-synthesized ZnO products in this work. The HPLC spectra during the photodegradation of phenol over the Eu(2.0 at%)/ZnO are shown in Fig. 7. The phenol showed a characteristic peak at retention time (RT) 5.6 min; it became weaker with the extended irradiation time and nearly disappeared after 30 min, indicating the excellent photocatalytic activity of the products. In addition to the above-mentioned main compound, the peaks at RT 1.1, 1.6, 2.2, 2.6 and 3.3 min could be assigned to muconic acid, pyrogallol, hydroquinone, resorcinol and benzoquinone intermediates, respectively when compared with the standard chemicals (Supplement Figs. S1–S5). This identification was also consistent with that reported in other studies [41–43]. The proposed photodegradation pathways are shown in Supplementary material Fig. S6, revealing hydroquinone, resorcinol and pyrogallol would be generated as by-products in the initial stage of the degradation [43]. It should also be noted that benzoquinone would

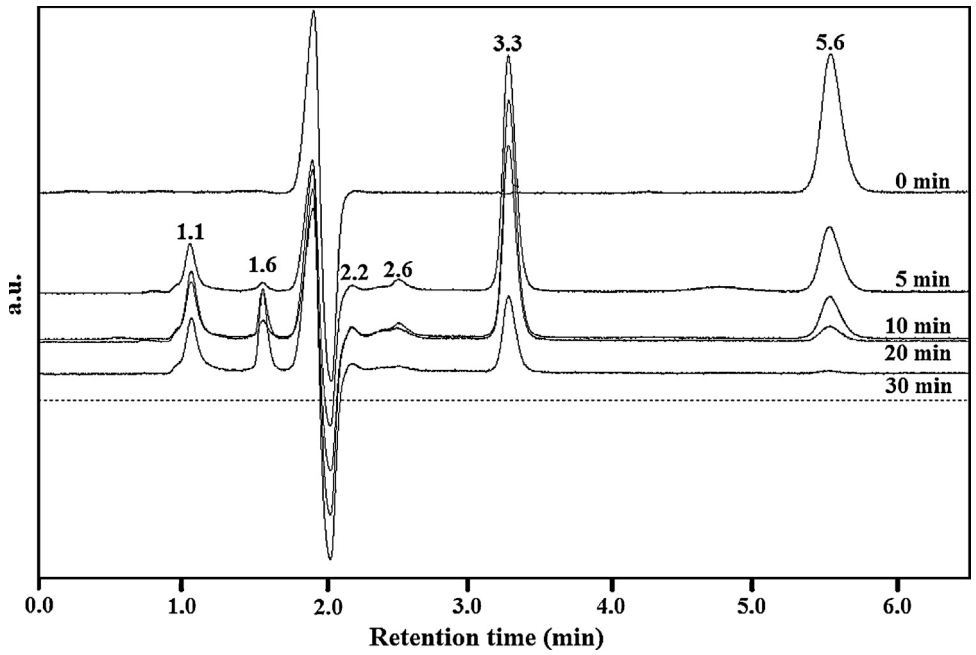

Fig. 7. Time-dependent HPLC chromatogram of phenol aqueous solution over the Eu(2.0 at%)/ZnO ([phenol] = 20 mg/L; volume of phenol = 100 mL; photocatalyst amount = 100 mg).

be generated due to dehydrogenation reaction of hydroquinone [44]. These aromatic intermediates would undergo ring cleavage reaction to yield aliphatic acids such as muconic acid, which would eventually convert to CO_2 and H_2O due to decarboxylation [42].

Fig. 8 shows that the degradation efficiency of Eu(2.0 at%)/ZnO reached 97.3% after 30 min irradiation. Under identical experimental conditions, the Eu(2.0 at%)/ZnO showed much higher activities than those of pure ZnO (62.7% degradation efficiency) and commercially available TiO_2 photocatalysts (40.8% degradation efficiency). For comparison, phenol degradation over Eu(2.0 at%)/ZNRs was also performed. It was clearly observed that only 70.4% phenol was degraded in the presence of Eu(2.0 at%)/ZNRs after 30 min irradiation. The increase in activity over Eu(2.0 at%)/ZnO compared to Eu(2.0 at%)/ZNRs was mainly attributed to the unique hierarchical porous surface structure and large surface area [4]. This view was confirmed by the N_2 adsorption–desorption analysis, as shown in Supplementary material Table S1 and Fig. S7, the surface area of Eu(2.0 at%)/ZnO was 22.6 m^2/g, which was more than 2.5 times that of the Eu(2.0 at%)/ZNRs (8.5 m^2/g). Further comparative experiments were also performed to evaluate the catalytic activity. It was shown that the concentration of phenol decreased only about 2.1% after 30 min irradiated in the absence of catalysts, and no observable change had been found for phenol with Eu(2.0 at%)/ZnO alone without exposure to light irradiation. Comparing the results of photolysis, adsorption and photocatalysis, this indicated that the phenol photocatalysis experiments were carried out at a nearly pure photocatalytic condition with negligible photolysis and adsorption.

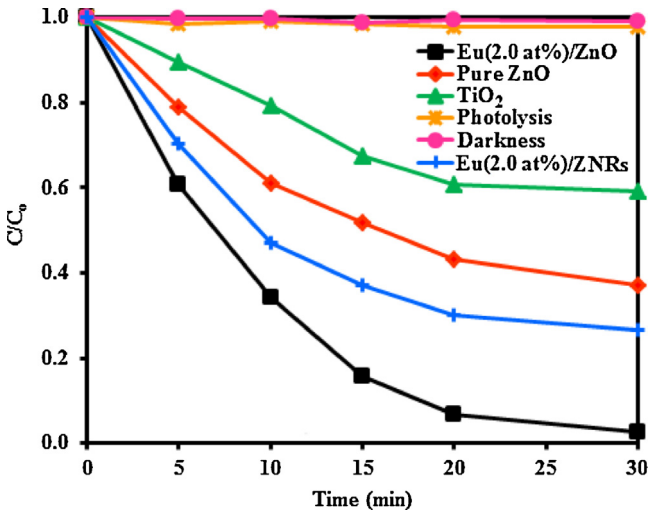

Fig. 8. Phenol concentration dependence on irradiation time using various photocatalysts ([phenol] = 20 mg/L; volume of phenol = 100 mL; photocatalyst amount = 100 mg).

3.3.1. *Effect of Eu doping content*

The degradation of phenol in the presence of Eu/ZnO with different Eu doping contents was measured and the results are shown in Fig. 9a. As can be seen, all the products of Eu/ZnO demonstrated higher photocatalytic activities than that of pure ZnO. Especially, Eu/ZnO with a Eu content of 2.0 at% exhibited the best performance on the photodegradation of phenol among the five products. At low Eu content (≤2.0 at%), the photocatalytic activities of the Eu/ZnO increased gradually with an increase in the Eu content. However, with increasing Eu content to 3.0 at%, the photocatalytic activities of the products decreased.

Fig. 9b shows the kinetic studies of the degradation of phenol over the Eu/ZnO with different Eu doping contents. It was observed that the photocatalytic reactions of phenol obeyed the pseudo-first-order kinetics according to the Langmuir–Hinselwood model and may be expressed as [17]:

$$ln\left(\frac{C_0}{C}\right) = kt \quad (4)$$

where k is the observed rate constant, C_o is the equilibrium concentration of phenol and C is the concentration at time t. Furthermore, according to the kinetics model, the k of different Eu/ZnO products and pure ZnO were calculated and summarized in Table 1. The results clearly demonstrated that the optimum Eu doping content was 2.0 at% with a k value of 0.1236 min^{-1}, which was 3.3 times larger than that of pure ZnO. The order of k value was also found

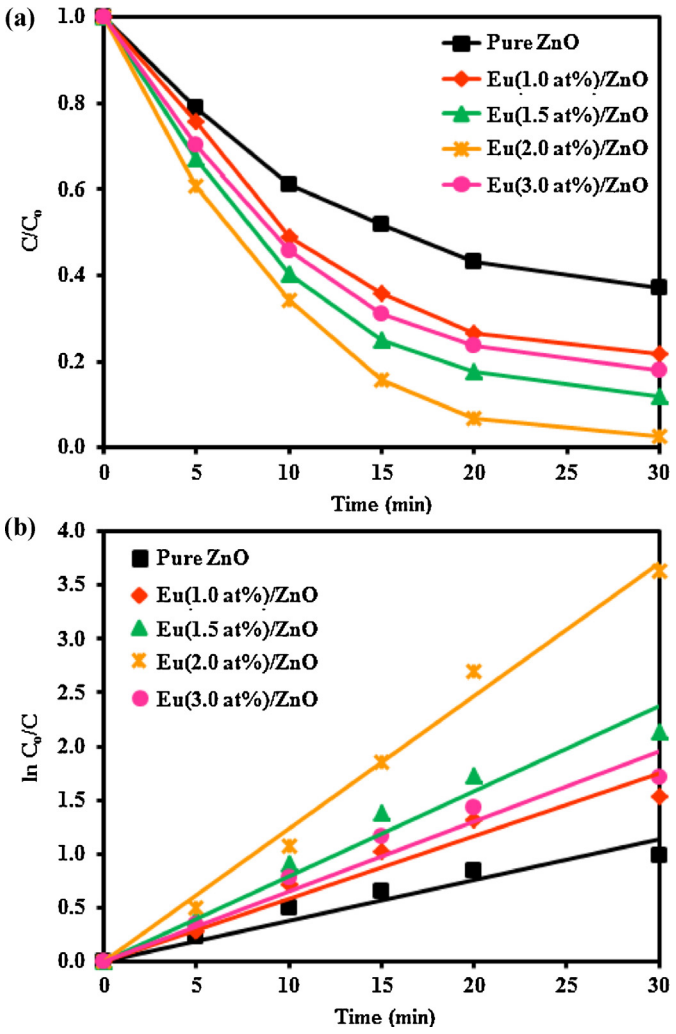

Fig. 9. (a) Effect of Eu doping content in Eu/ZnO on phenol degradation ([phenol] = 20 mg/L; volume of phenol = 100 mL; photocatalyst amount = 100 mg) and (b) Pseudo-first-order linear plots of $\ln(C_0/C)$ versus irradiation time for the degradation kinetics of phenol using different photocatalysts.

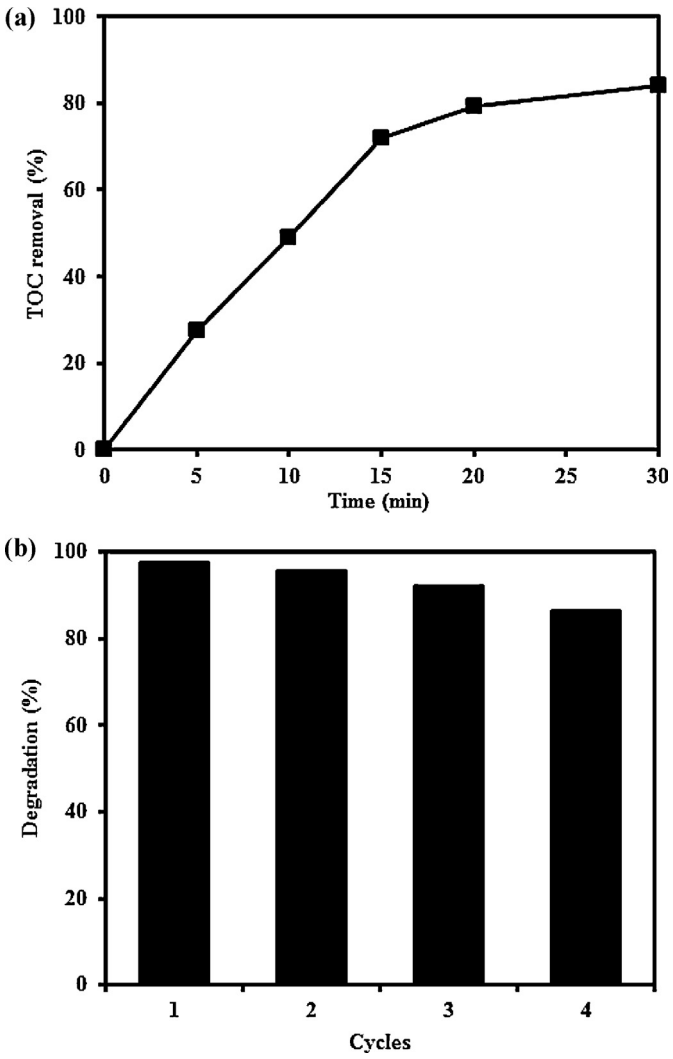

Fig. 10. (a) TOC removal in the presence of Eu(2.0 at%)/ZnO under natural sunlight irradiation ([phenol] = 20 mg/L; volume of phenol = 100 mL; photocatalyst amount = 100 mg) and (b) Recycling efficiency of Eu(2.0 at%)/ZnO.

to be 2.0 > 1.5 > 3.0 > 1.0 > 0.0 at%, which was consistent with the results shown in Fig. 9a. As for enhancement of the photocatalytic activity of the Eu/ZnO, it will be discussed in detail below.

3.3.2. TOC removal and catalyst recycle

The TOC concentration was chosen as a mineralization index to characterize the phenol degradation. The time independence of the TOC data in the phenol solution over the Eu(2.0 at%)/ZnO product under natural sunlight irradiation is shown in Fig. 10a. It showed that the TOC concentration decreased gradually with reaction time as the phenol degraded. The maximum TOC removal was 83.9% after 30 min of irradiation, revealing that most of the phenol was mineralized during the photocatalytic process, which was important for the practical applications of Eu(2.0 at%)/ZnO photocatalysts to avoid secondary pollution.

Furthermore, the ease with which the catalyst could be separated from a suspended solution after a reaction was also important for its practical applications. Due to the relatively larger size, the microsphere morphology of the product has an advantage over other nanostructured catalysts, as the product can achieve the easy solid/liquid separation. To investigate the stability of the photoactivity for the as-synthesized products, cyclic experiments were carried out under the same experimental conditions. As shown in Fig. 10b, the photocatalytic activities of Eu(2.0 at%)/ZnO did not exhibit any significant loss after four recycling runs. The slight decrease in activity can be attributed to catalyst loss because it was very difficult to avoid no any loss of catalyst materials in the experiments. XRD analysis of the Eu(2.0 at%)/ZnO after the fourth catalytic reaction in Supplementary material Fig. S8 showed that the crystal structure of the used Eu(2.0 at%)/ZnO still well maintained after recycling test, indicating the stability of the photocatalyst. The results of the TOC removal efficiency and good stability showed that the Eu(2.0 at%)/ZnO synthesized by this facile method was promising in the practical application of photocatalytic degradation of organic pollutants.

3.4. Possible photocatalytic mechanism

3.4.1. Photoluminescence emission spectra

In order to determine the fate of photogenerated electron-hole pairs in the products and understand the photocatalytic mechanism, the PL emission spectra were performed. Generally, a higher PL intensity indicated a higher photogenerated electron-hole recombination rate and decreased the reaction chance of photogenerated charge carriers. On the other hand, a lower PL intensity implied a lower photogenerated electron-hole recombination rate, revealing more photogenerated electrons and holes

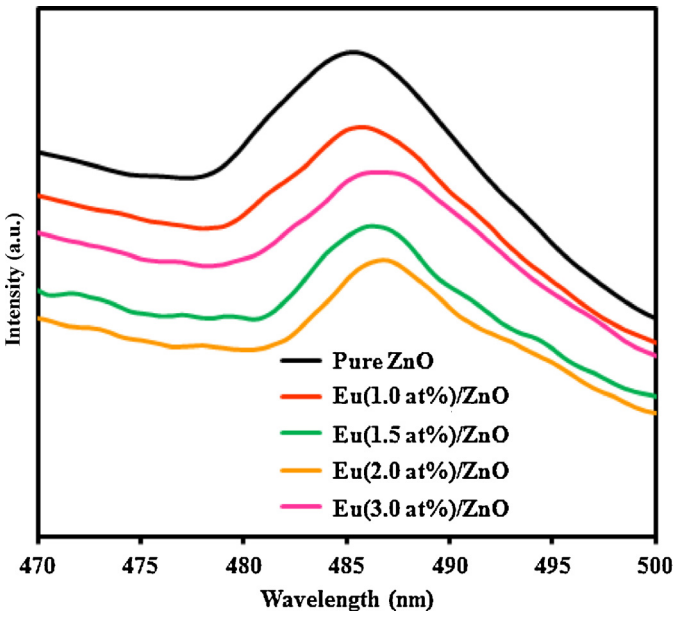

Fig. 11. PL spectra of pure ZnO and Eu/ZnO with different doping contents of Eu.

can participate in the oxidation and reduction reactions and consequently improved the photocatalytic performance [45].

Fig. 11 shows the PL spectra of Eu/ZnO with different contents of Eu when the excitation wavelength was 325 nm. It can be observed that the pure ZnO has the highest PL intensity, while the Eu(2.0 at%)/ZnO has the lowest PL intensity. Such PL results were consistent with the photocatalytic activity of the products. According to Štengl et al. [32], the value of the space charge region potential for an efficient separation of the photogenerated charge carriers had a lower limit. As the doping content of Eu increased (<2.0 at%), the surface barrier became higher and the space charge region became narrower. The photogenerated electron-hole pairs within the region were thus efficiently separated by the large electric field before recombination which led to the lower PL intensity and caused an increase in the photocatalytic activity. However, when the doping content was high (>2.0 at%), the space charge layer became very narrow and the penetration depth of light into ZnO greatly exceeded the space charge layer; therefore the recombination of the photogenerated electron-hole pairs became easier, which increased the PL intensity and retarded the photocatalytic activity of ZnO for phenol degradation.

3.4.2. Active species responsible for phenol degradation

As literature documented [1,3], a large number of main active species including h_{vb}^+, •OH and $O_2^{\bullet-}$ were involved in the photocatalytic process. Therefore, the effects of different scavengers on the degradation of phenol were investigated in an attempt to elucidate the photocatalytic mechanism. In this study, ethanol and acetonitrile were introduced to the reaction system as •OH scavenger [46,47], sodium iodide (NaI) was added as a scavenger of h_{vb}^+ [48] and *p*-benzoquinone (BQ) was adopted to quench $O_2^{\bullet-}$ [49]. As a consequence of quenching, the photocatalytic reaction of phenol degradation will be suppressed. The extent of decrease in the phenol degradation efficiency that induced by the scavenger, indicating the importance of the corresponding active species.

Fig. 12a shows that the degradation efficiency of phenol decreased significantly from 97.3% to 65.2% after 30 min irradiation when ethanol was added into the photocatalytic reaction solution, reflecting the participation of •OH in the reaction mechanism. Differently, when NaI and BQ were added, it decreased to 87.1% and 94.2%, respectively in the same duration, revealing that

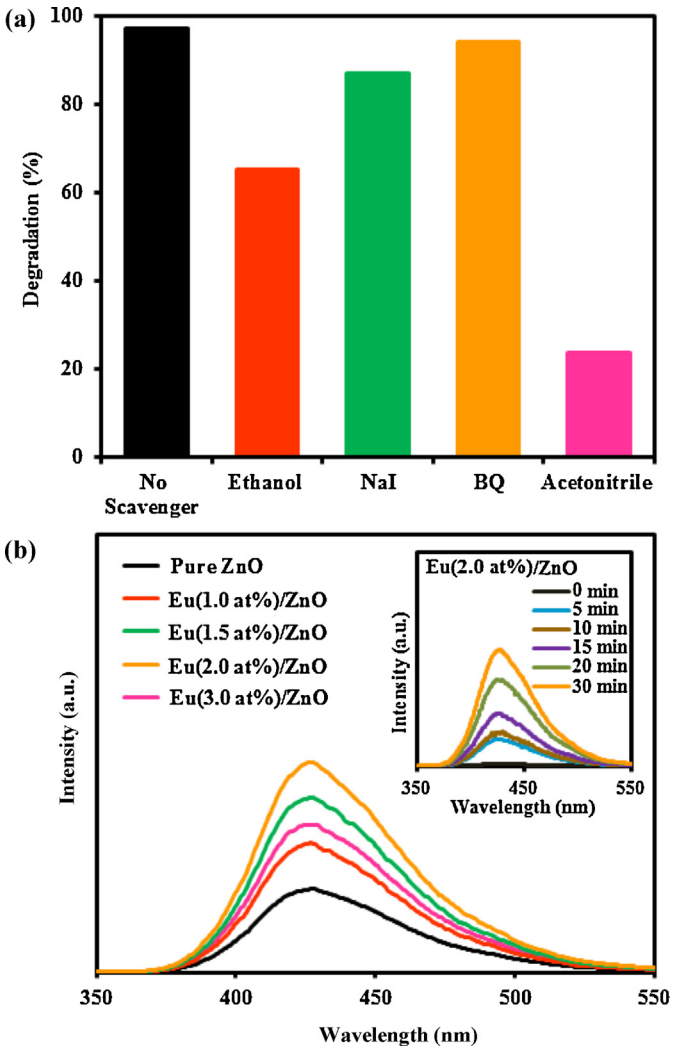

Fig. 12. (a) Effects of different scavengers on degradation of phenol in the presence of Eu(2.0 at%)/ZnO ([phenol] = 20 mg/L; volume of phenol = 100 mL; photocatalyst amount = 100 mg) and (b) PL spectra of the aqueous basic solution of terephthalic acid with an excitation at 315 nm under different products for 30 min. Inset of (b) is the PL spectra changing with irradiation time for the case of the Eu(2.0 at%)/ZnO.

h_{vb}^+ and $O_2^{\bullet-}$ contributed to lesser extent in phenol degradation. Furthermore, acetonitrile, an extremely stable molecule was used to replace water as a solvent in order to discern the participation of •OH or h_{vb}^+ in the photocatalytic reaction mechanism. A non-aqueous reaction medium ruled out the participation of •OH that formed by water getting trapped in the hole in the oxidation process [47]. The results showed that when the reaction was performed without water (100% acetonitrile), the reaction was largely inhibited, indicating the •OH were the main active species responsible for phenol degradation.

The formation of •OH on the sunlight irradiated ZnO products was further confirmed by the TA-PL technique. The PL emission spectra of different ZnO products excited at 315 nm from terephthalic solution were measured after 30 min irradiation. The result showed that an obvious PL signal at about 425 nm was observed, revealing that •OH radicals were formed during the photocatalytic reactions, which was consistent with the results in Fig. 12a. The peak intensity of different photocatalysts is shown in Fig. 12b. It was clear that the formation rate of •OH on the Eu(2.0 at%)/ZnO was higher than that of other products. This implied that the former has higher photocatalytic activity than the latter, which was also agreed well with the results of PL emission spectra in Fig. 11. Moreover, all

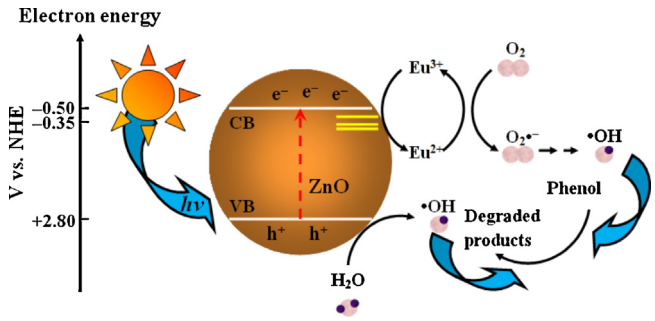

Scheme 2. Possible photocatalytic mechanism of Eu/ZnO.

the Eu/ZnO exhibited higher PL intensity than pure ZnO, suggesting that doping of Eu on ZnO was a good route to accelerate the interfacial charge transfer and inhibit the recombination of electron-hole pairs, which resulted in the increase of •OH formation.

In addition, the inset of Fig. 12b shows the change of PL spectra with irradiation time for the case of Eu(2.0 at%)/ZnO. A gradual increase in PL intensity was observed with increasing irradiation time, which suggested that the fluorescence was caused by chemical reactions of terephthalic acid with •OH formed during photoilluminated reactions. Therefore, these results confirmed the evidence of •OH formation and indeed participated in degradation process.

3.4.3. *Possible degradation mechanism and the role of Eu dopant*

Combining our experiment results with the related literatures [1,3,32], a postulated mechanism for the enhanced photocatalysis of Eu/ZnO could be proposed in Scheme 2. Under the irradiation, the electrons (e_{cb}^-) are excited from the valence band to the conduction band of ZnO leaving behind h_{vb}^+. According to the standard redox potentials of $E^0(Eu^{3+}/Eu^{2+}) = -0.35$ V, $E^0(O_2/O_2^{\bullet-}) = -0.33$ V and $E_{vb}(ZnO) = -0.50$ V versus NHE [50,51], the presence of Eu^{3+} with partially filled f-orbital in ZnO being strong Lewis acid can effectively trap the e_{cb}^- and inhibit the recombination with h_{vb}^+. The reduced state of Eu^{2+} ions are very instable so that the e_{cb}^- can be easily detrapped and transferred to the O_2 molecules promoting the $O_2^{\bullet-}$ formation and then converted to active •OH. This suggested that the Eu dopant can serve as an effective charge carrier trap and facilitated the excited e_{cb}^- transfer under natural sunlight irradiation. The degradation mechanism for the Eu/ZnO can be given as [48,52]:

$$ZnO + h\nu \rightarrow ZnO(e_{cb}^- + h_{vb}^+) \quad (5)$$

$$Eu^{3+} + e_{cb}^- \rightarrow Eu^{2+} \text{ (electrontrapping)} \quad (6)$$

$$Eu^{2+} + O_2 \rightarrow Eu^{3+} + O_2^{\bullet-} \text{ (electrontransfer)} \quad (7)$$

$$O_2^{\bullet-} + H^+ \rightarrow {}^{\bullet}OOH \quad (8)$$

$$^{\bullet}OOH + H^+ + e_{cb}^- \rightarrow H_2O_2 \quad (9)$$

$$H_2O_2 + e_{cb}^- \rightarrow {}^{\bullet}OH + OH^- \quad (10)$$

At the same time, the photogenerated h_{vb}^+ can be captured on the catalyst surface undergoing charge transfer with adsorbed water molecules or with surface-bound hydroxide species to generate active •OH as shown in steps:

$$h_{vb}^+ + H_2O \rightarrow H^+ + {}^{\bullet}OH \quad (11)$$

$$h_{vb}^+ + OH^- \rightarrow {}^{\bullet}OH \quad (12)$$

Thus, the separation of the charge carriers was attributed to such trapping by Eu dopant in ZnO. Subsequently, enhanced the yield of •OH quantities in the degradation of phenol, which further improved the photocatalytic activity of Eu/ZnO.

4. Conclusions

In the absence of any surfactants or structure-directing reagents, Eu-doped ZnO hierarchical micro/nanospheres (Eu/ZnO) with different doping contents of Eu were successfully obtained by a facile chemical solution route and confirmed by XRD, FESEM, EDX, TEM, HRTEM, XPS, UV–vis DRS, N_2 adsorption–desorption and PL measurements. The proposed method was rather simple, mild, cost-effective and particularly suited for industrial production of Eu/ZnO. The investigation of photocatalytic ability showed that the Eu/ZnO activity was greatly influenced by the Eu doping content. At an optimal Eu doping content of 2.0 at%, the phenol degradation reached 97.3% within 30 min natural sunlight irradiation and exhibited much higher photocatalytic activity than those of pure ZnO, Eu(2.0 at%)/ZNRs and commercial TiO_2. The photocatalytic enhancement of Eu/ZnO was attributed to the high charge separation efficiency and •OH generation ability as evidenced by the PL spectra. The •OH was determined as main active species during the photocatalytic degradation process. Moreover, the as-synthesized Eu/ZnO exhibited a high mineralization capacity of phenol and could be easily recycled without any significant loss of the photocatalytic activity, which were favorable for the potential practical applications.

Acknowledgments

This research was supported by a Research Universiti grant (no. 814176) and a Post Graduate Research Scheme (no. 8045032) from Universiti Sains Malaysia as well as a My PhD scholarship through Malaysia Government.

Appendix A. Supplementary data

Supplementary data associated with this article can be found, in the online version, at http://dx.doi.org/10.1016/j.apcatb.2013.11.001.

References

[1] J.C. Sin, S.M. Lam, A.R. Mohamed, K.T. Lee, Int. J. Photoenergy 2012 (2012) 185159.
[2] H.Q. Sun, X.H. Feng, S.B. Wang, H.M. Ang, M.O. Tadé, Chem. Eng. J. 170 (2011) 270–277.
[3] S.M. Lam, J.C. Sin, A.Z. Abdullah, A.R. Mohamed, Desalin. Water Treat. 41 (2012) 131–169.
[4] H.B. Lu, S.M. Wang, L. Zhao, J.C. Li, B.H. Dong, Z.X. Xu, J. Mater. Chem. 21 (2011) 4228–4234.
[5] H. Ishiguro, R. Nakano, Y.Y. Yao, J.S. Kajioka, A. Fujishima, K. Sunada, M. Minoshima, K. Hashimoto, Y. Kubota, Photochem. Photobiol. Sci. 10 (2011) 1825–1829.
[6] J.F. Ma, J. Zou, L.Y. Li, C. Yao, T.L. Zhang, D.L. Li, Appl. Catal. B: Environ. 134–135 (2013) 1–6.
[7] T. Nakajima, T. Kitamura, T. Tsuchiya, Appl. Catal. B: Environ. 108–109 (2011) 47–53.
[8] Y.C. Wu, Y.C. Chaing, C.Y. Huang, S.F. Wang, H.Y. Yang, Dyes Pigments 98 (2013) 25–30.
[9] S.K. Kansal, A.H. Ali, S. Kapoor, Desalination 259 (2010) 147–155.
[10] R. Wahab, S.K. Tripathy, H.S. Shin, M. Mohapatra, J. Musarrat, A.A. Al-Khedhairy, N.K. Kaushik, Chem. Eng. J. 226 (2013) 154–160.
[11] A. Kajbafvala, H. Ghorbani, A. Paravar, J.P. Samberg, E. Kajbafvala, S.K. Sadrnezhaad, Superlattice Microst. 51 (2012) 512–522.
[12] J.C. Sin, S.M. Lam, K.T. Lee, A.R. Mohamed, Ceram. Int. 39 (2013) 5833–5843.
[13] S.M. Lam, J.C. Sin, A.Z. Abdullah, A.R. Mohamed, Mater. Lett. 93 (2013) 423–426.
[14] J.F. Li, G.Z. Lu, Y.Q. Wang, Y. Guo, Y.L. Guo, J. Colloid Interf. Sci. 377 (2012) 191–196.
[15] C.L. Ren, B.F. Yang, M. Wu, J. Xu, Z.P. Fu, Y. Lv, T. Guo, Y.X. Zhao, C.Q. Zhu, J. Hazard. Mater. 182 (2010) 123–129.

[16] O. Yayapao, T. Thongtem, A. Phuruangrat, S. Thongtem, Mater. Lett. 90 (2013) 83–86.
[17] S.M. Lam, J.C. Sin, A.Z. Abdullah, A.R. Mohamed, Ceram. Int. 39 (2013) 2343–2352.
[18] M. Khatamian, A.A. Khandar, B. Divband, M. Haghighi, S. Ebrahimiasl, J. Mol. Catal. A: Chem. 365 (2012) 120–127.
[19] C. Karunakaran, P. Gomathisankar, G. Manikandan, Mater. Chem. Phys. 123 (2010) 585–594.
[20] S.M. Lam, J.C. Sin, A.Z. Abdullah, A.R. Mohamed, J. Mol. Catal. A: Chem. 370 (2013) 123–131.
[21] J.H. Yang, X. Li, J.H. Lang, L.L. Yang, M.B. Wei, M. Gao, X.Y. Liu, H.J. Zhai, R. Wang, Y. Liu, J. Cao, Mater. Sci. Semicond. Process. 14 (2011) 247–252.
[22] Y.P. Du, Y.W. Zhang, L.D. Sun, C.H. Yan, J. Phys. Chem. C 112 (2008) 12234–12241.
[23] S. Anandan, A. Vinu, T. Mori, N. Gokulakrishnan, P. Srinivasu, V. Murugesan, K. Ariga, Catal. Commun. 8 (2007) 1377–1382.
[24] Y. Zhou, S.X. Lu, W.G. Xu, Environ. Prog. Sustain. Energy 28 (2009) 226–233.
[25] R. John, R. Rajakumari, Nano-Micro Lett. 4 (2012) 65–72.
[26] S.W. Liu, C. Li, J.G. Yu, Q.J. Xiang, CrystEngComm 13 (2011) 2533–2541.
[27] J.G. Yu, X.X. Yu, Environ. Sci. Technol. 42 (2008) 4902–4907.
[28] M. Fu, Y.L. Li, S.W. Wu, P. Lu, J. Liu, F. Dong, Appl. Surf. Sci. 258 (2011) 1587–1591.
[29] A. Prakash, S.K. Misra, D. Bahadur, Nanotechnology 24 (2013) 095705.
[30] A.P. Zhang, J.Z. Zhang, J. Hazard. Mater. 173 (2010) 265–272.
[31] Y. Uwamino, T. Ishizuka, J. Electron. Spectrosc. Relat. Phenom. 34 (1984) 67–78.
[32] V. Štengl, S. Bakardjieva, N. Murafa, Mater. Chem. Phys. 114 (2009) 217–226.
[33] S. Anandan, M. Miyauchi, Phys. Chem. Chem. Phys. 13 (2011) 14937–14945.
[34] C. Wang, Y.H. Ao, P.F. Wang, J. Hou, J. Qian, Appl. Surf. Sci. 257 (2010) 227–231.
[35] Q.Y. Li, E.B. Wang, S.H. Li, C.L. Wang, C.G. Tian, G.Y. Sun, J.M. Gu, R. Xu, J. Solid State Chem. 182 (2009) 1149–1155.
[36] Y.F. Gao, K. Koumoto, Cryst. Growth Des. 5 (2005) 1983–2017.
[37] J.C. Sin, S.M. Lam, A.R. Mohamed, Korean J. Chem. Eng. 28 (2011) 84–92.
[38] K. Schmidt-Bäumler, Th. Heberer, H.J. Stan, Acta Hydrochim. Hydrobiol. 27 (1999) 143–149.
[39] W.J. Zhong, D.H. Wang, X.W. Xu, Q. Luo, B.Y. Wang, X.Q. Shan, Z.J. Wang, Chemosphere 80 (2010) 998–1005.
[40] J.K. Fawell, S. Hunt, Environmental Toxicology: Organic Pollutants, Ellis Horwood Limited, Chichester, 1988.
[41] P. Górska, A. Zaleska, J. Hupka, Sep. Purif. Technol. 68 (2009) 90–96.
[42] A. Sobczyński, Ł. Duczmal, W. Zmudziński, J. Mol. Catal. A: Chem. 213 (2004) 225–230.
[43] Z.F. Guo, R.X. Ma, G.J. Li, Chem. Eng. J. 119 (2006) 55–59.
[44] J. Villaseñor, P. Reyes, G. Pecchi, Catal. Today 76 (2002) 121–131.
[45] H.J. Liu, G.G. Liu, Q.X. Zhou, G.H. Xie, Z.H. Hou, M.L. Zhang, Z.W. He, Microporous Mesoporous Mater. 142 (2011) 439–443.
[46] B. Abramović, D. Šojić, V. Despotović, D. Vione, M. Pazzi, J. Csanádi, Appl. Catal. B: Environ. 105 (2011) 191–198.
[47] Y.X. Chen, S.Y. Yang, K. Wang, L.P. Lou, J. Photochem. Photobiol. A: Chem. 172 (2005) 47–54.
[48] X.F. Chang, J. Huang, Q.Y. Tan, M. Wang, G.B. Ji, S.B. Deng, G. Yu, Catal. Commun. 10 (2009) 1957–1961.
[49] P.F. Ji, J.L. Zhang, F. Chen, M. Anpo, Appl. Catal. B: Environ. 85 (2009) 148–154.
[50] Y.J. Wang, R. Shi, J. Lin, Y.F. Zhu, Energy Environ. Sci. 4 (2011) 2922–2929.
[51] Y.B. Xie, C.W. Yuan, Mater. Res. Bull. 39 (2004) 533–543.
[52] H. Xu, H.M. Li, L. Xu, C.D. Wu, G.S. Sun, Y.G. Xu, J.Y. Chu, Ind. Eng. Chem. Res. 48 (2009) 10771–10778.